Time-bin modulated polarization-entangled biphotons from cavity-enhanced down-conversion

Christopher E. Kuklewicz,* Franco N. C. Wong, and Jeffrey H. Shapiro
Massachusetts Institute of Technology
(Dated: February 1, 2008)

We have generated a new type of biphoton state by cavity-enhanced down-conversion in a type-II phase-matched, periodically-poled $KTiOPO_4$ (PPKTP) crystal. By introducing a weak intracavity birefringence, the polarization-entangled output was modulated between the singlet and triplet states according to the arrival-time difference of the signal and idler photons. This cavity-enhanced biphoton source is spectrally bright, yielding a single-mode fiber-coupled coincidence rate of 0.7 pairs/s per mW of pump power per MHz of down-conversion bandwidth. Its novel biphoton behavior may be utilized in sensitive measurements of weak intracavity birefringence.

PACS numbers: 42.65.Lm, 03.65.Ud, 03.67.Mn, 42.50.Dv

Spontaneous parametric down-conversion (SPDC) is the principal source for polarization-entangled photon pairs [1], but its ∼THz bandwidth makes it ill-suited for coupling to the ∼MHz bandwidth of an atomic absorption line. What is needed, to make such coupling efficient, is a bright, narrowband source of polarization-entangled photons [2]. Ou and Lu [3] used an optical cavity to increase the efficiency and narrow the bandwidth of a continuous-wave (cw) type-I phase-matched down-converter. Wang *et al.* [4] did the same for a pair of cw type-I down-converters, one rotated by 90°, in a ring cavity to produce polarization-entangled photons. We will report the first cavity-enhanced operation of a cw type-II down-converter, resulting in a spectrally bright, narrowband source of frequency-degenerate polarization-entangled photon pairs. More importantly, by controlling a weak intracavity birefringence, our source generates a new type of biphoton state whose polarization-entangled output is modulated between the singlet and triplet states according to the arrival-time difference between the signal and idler photons.

Consider conventional cw SPDC in a collinear configuration that is type-II phase matched at frequency degeneracy. The post-selected biphoton state emerging from a 50-50 beam splitter placed after the usual timing-compensation crystal is then $|\psi\rangle = (|H\rangle_1|V\rangle_2 + e^{i\phi}|V\rangle_1|H\rangle_2)/\sqrt{2}$, in the horizontal-vertical (H-V) basis, where the subscripts label the beam splitter output ports. Ordinarily we have $\phi = 0$, so $|\psi\rangle$ is a triplet, but a half-wave plate in one of the output paths can transform $|\psi\rangle$ to a singlet by making $\phi = \pi$. The situation becomes more complicated—and more interesting—when that down-converter is embedded in a single-ended cavity that resonates the signal and idler. If the signal and idler photons resulting from down-conversion of a pump photon emerge from the output coupler after the same number of roundtrips within the cavity, then they yield a triplet for the post-selected biphoton state. However, the times at which these photons leave the cavity may differ by integer multiples of the cavity roundtrip time, τ_c. Taking τ_c as a natural time-bin unit for the system, we have that the biphoton state associated with a photon pair whose arrival-time difference is $m\tau_c$ is $|\psi\rangle = (|H\rangle_1|V\rangle_2 + e^{im\phi}|V\rangle_1|H\rangle_2)/\sqrt{2}$, where ϕ is the roundtrip cavity birefringence. By tuning the cavity birefringence to achieve $\phi \neq 0$—something that is easily done with type-II phase matching—we get a new type of biphoton, which exhibits time-bin modulated polarization entanglement. When $\phi = \pi$ and m is even, this biphoton is a triplet; when $\phi = \pi$ and m is odd, it is a singlet. Before describing our experimental work, we shall provide a more precise characterization of cavity-enhanced type-II SPDC.

Consider the cw down-conversion configuration shown in Fig. 1. A length-L KTP intracavity compensating crystal (ICC) and a length-L PPKTP crystal are contained inside a single-ended optical cavity, and a length-$L/2$ KTP external compensating crystal (ECC) is employed outside the cavity. The cavity mirrors do not reflect the frequency-ω_P pump, but they do resonate the frequency-degenerate signal and idler. The pump propagates along the x-axes of all three crystals. The y-axis of the PPKTP crystal is horizontal, and the y-axes of the compensating crystals are vertical. Without the cavity mirrors, ICC has no effect; with the cavity mirrors, ICC provides timing compensation for photons that perform one or more roundtrips before exiting the cavity.

Our experiments measured statistics of the time difference, τ, between photon detections made in the H-V or the ±45° polarization bases. The H-V coincidence rate is $R_{HV}(\tau) = C|K_{SI}^{(p)}(\tau)|^2$ in terms of the phase-sensitive correlation of the signal and idler, $K_{SI}^{(p)}(\tau)$, and a proportionality constant C, and the ±45° rate is $R_{\pm 45}(\tau) = C|K_{SI}^{(p)}(\tau) - K_{SI}^{(p)}(-\tau)|^2/4$. Furthermore, we have [5] $K_{SI}^{(p)}(\tau) \propto \sum_{m=-\infty}^{\infty}\sum_{\ell=0}^{\infty} R^{\ell+|m|/2} e^{im\phi/2}\mathrm{box}_{\tau_0}(\tau - m\tau_c)$, at a signal-idler double resonance, where R is the output coupler's reflectivity. Also, $\mathrm{box}_{\tau_0}(\tau) = 1$ for $|\tau| \leq \tau_0/2 \equiv |\Delta k'|L/2$ and zero otherwise, which is the time-domain manifestation of the phase-matching function,

*Electronic address: chrisk@alum.mit.edu

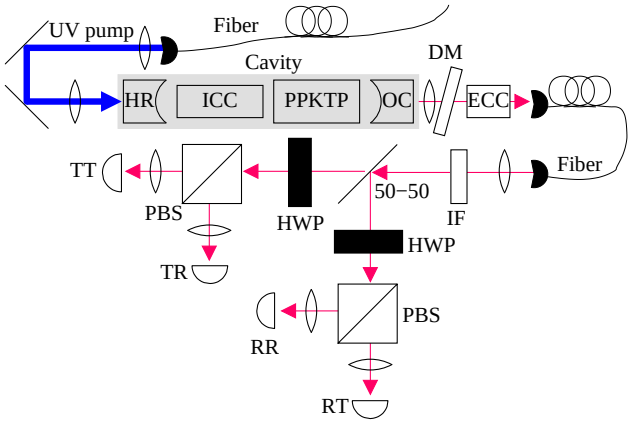

FIG. 1: (Color online) Cavity-enhanced SPDC setup. HR, high reflector; ICC, intracavity compensating crystal; ECC, external compensating crystal; OC, output coupler; HWP half-wave plate; PBS polarizing beam splitter; DM, dichroic mirror; IF, interference filter; TT, TR, RT, and RR, single-photon detectors.

with $\Delta k'$ being the frequency derivative of the phase mismatch. In our experiment, $\tau_0 \approx 3.5\,\mathrm{ps}$, $\tau_c \approx 826\,\mathrm{ps}$, and ϕ was controlled by temperature tuning of the ICC. Setting $R = 0$ reduces $K_{SI}^{(p)}(\tau)$ to the SPDC result, i.e., the $\ell = m = 0$ term. For $R > 0$, the $m \neq 0$ terms are due to correlations between signal and idler photons that came from the same pump photon but exited the output coupler with the signal photon having taken m more cavity roundtrips than the idler did and incurring m times the cavity birefringence. Because the different box functions in $K_{SI}^{(p)}(\tau)$ are nonoverlapping in our experiment, we find that $R_{HV}(\tau) = \sum_{m=-\infty}^{\infty} R_{HV}^{(m)}(\tau)$ and $R_{\pm 45}(\tau) = \sum_{|m|=0}^{\infty} \sin^2(m\phi/2) R_{HV}^{(|m|)}(\tau)$, where $R_{HV}^{(m)}(\tau)$ is the $\mathrm{box}_{\tau_0}(\tau - m\tau_c)$ term in the H-V coincidence rate.

Our experimental setup is shown in Fig. 1. The intracavity compensating crystal was unpoled KTP polished to a length within $\pm 1\mu$m of the ∼9.7-mm-long PPKTP crystal, as verified by birefringence measurements made with a tunable laser. Each was placed on its own thermoelectric cooler for independent temperature control with 0.01°C stability. The PPKTP crystal was tuned to frequency degeneracy for SPDC, and the ICC was tuned to control the cavity birefringence. The PPKTP, ICC, and ECC crystals were antireflection coated at 795 nm and 397.5 nm. The ICC and PPKTP were placed inside an optical cavity formed by an input mirror, coated for high reflection at 795 nm and an output coupler that was coated for 92% reflection at 795 nm; both mirrors were also high transmission at 397 nm. The mirrors had 50 mm radii of curvature and were separated by 104.9 mm, which yielded a ∼1.21 GHz free spectral range ($\tau_c \approx 826\,\mathrm{ps}$). The output coupler was mounted on a piezoelectric transducer for cavity-length control.

We used a cw external-cavity diode laser (Toptica) as the pump source, operated near 397.5 nm. The pump light was sent through 2 m of single-mode fiber (StockerYale) that served as a spatial filter, and ∼1 mW of power was mode matched into the cavity. Most of the pump light passed through the cavity and was then diverted from the output path by the dichroic mirror (DM). The cavity finesse at 795 nm was measured to be ∼55, corresponding to 11% loss per roundtrip, which was consistent with the 92% reflectivity of the output coupler and the ∼0.3% loss per surface for the crystals. A ∼5 mm KTP external compensating crystal was placed outside of the cavity before the aspheric lens that coupled the down-converted light into a single-mode fiber equipped with polarization-control paddles. The resonantly generated down-converted light had a well defined spatial mode that allowed efficient mode matching into a single-mode fiber. After the fiber there was a 1 nm interference filter (IF) and a 50-50 beam splitter. The transmitted arm contained a half-wave plate (HWP) set at θ_T and a polarizing beam splitter (PBS) whose transmitted and reflected paths led to single-photon counters TT and TR, respectively. The reflected path from the 50-50 beam splitter contained another HWP (set at θ_R) and a PBS with two detectors (RT and RR) in its output paths. The single-photon detectors were all PerkinElmer silicon avalanche photodiodes. Weak pump-beam reflections (∼17%) at the cavity mirrors created a weak pump modulation as the cavity length was swept.

We measured the coincidence rates between the TT and TR detectors and between the RT and RT detectors. TT and TR detections were also used to provide start and stop signals for collecting arrival-time-difference histograms for comparison with the predicted behavior of $R_{HV}(\tau)$ and $R_{\pm 45}(\tau)$. The RT and RR measurements were always made with $\theta_R = 0$, corresponding to the H-V basis (aligned to the PPKTP's y and z axes). Thus they monitored the maximum coincidence rate to check that the down-conversion remained consistent during data collection. The TT-TR coincidence rate and arrival-time difference histogram were measured either with $\theta_T = 0$ (for the H-V basis) or with $\theta_T = \pi/8$ (for the ±45° basis). Data were collected while the cavity length was swept through one free spectral range (FSR) using a 40-s-period triangular waveform. The arrival-time-difference histograms at a signal-idler double resonance, shown in the figures below, come from 16 minutes of data integration using 38.3 ps time bins. Had the cavity length been locked at a double resonance, the data collection time would have been significantly reduced.

We measured the cavity transmission of a ∼795 nm probe beam and tuned the temperature of the ICC to simultaneously resonate both polarizations as the cavity length was swept, after which the probe laser was removed and SPDC coincidence counting was performed. The resulting TT-TR data are shown in Fig. 2, corresponding to the case of zero birefringence, $\phi = 0$. The upper curve is the arrival-time-difference histogram for the H-V basis. Its peaks are separated by the ∼826 ps cavity roundtrip time τ_c, and broadened—from their

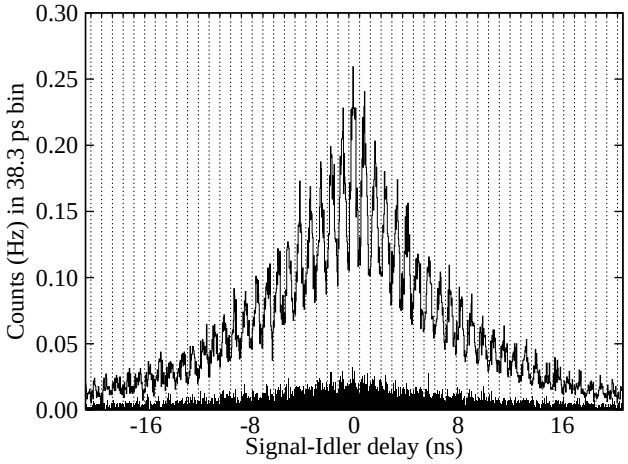

FIG. 2: Arrival-time-difference histograms averaged over 16 minutes. Upper curve is for the H-V basis. The lower filled curve is for the $\pm 45^\circ$ basis.

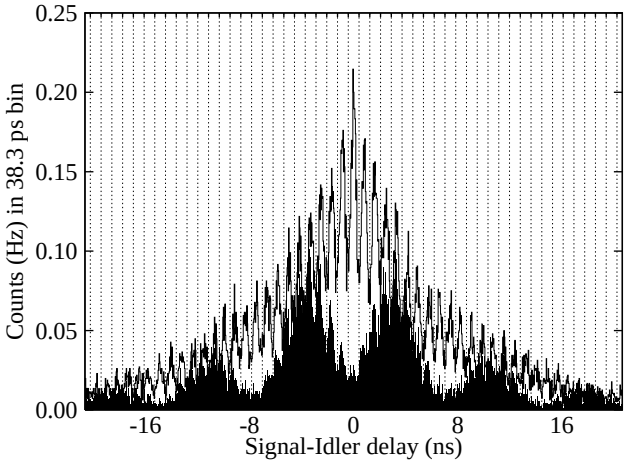

FIG. 3: Similar to Fig. 2 with temperature detuned by 0.53°C

3.5 ps theoretical width—by the 350 ps time jitter of our single-photon counters. Its highest ($\tau = 0$) peak was due to signal-idler pairs that exited the cavity after the same number of roundtrips. The filled curve in Fig. 2 is the arrival-time-difference histogram for the $\pm 45^\circ$-basis. Figure 5 fill A shows the ratio of $\pm 45^\circ$-basis coincidences, summed over the peak for each m value, to the corresponding sum for H-V-basis coincidences, after a small background-count correction has been made (0.014 Hz/bin for H-V and 0.009 Hz/bin for $\pm 45^\circ$). The ratio of the total of the central 41 peaks in the $\pm 45^\circ$ histogram to that for the H-V histogram was 0.131. This corresponds to a quantum-interference fringe visibility of 76.8%, indicating that the SPDC output is in a polarization-entangled triplet state [6]. Much of the loss from ideal visibility can be attributed to the reflected pump light, as discussed below. The slight curvature seen in Fig. 5 fill A can be attributed to temperature fluctuations of the ICC that were equivalent to an offset of 0.004° C from the ideal value.

By varying the ICC temperature, while keeping the PPKTP temperature fixed, we were able to control the cavity birefringence precisely. At zero birefringence, the effective lengths of the ICC and PPKTP were the same. By varying the ICC temperature, the effective lengths could be tuned to achieve $\phi = 2\pi T/T_{2\pi}$, where T is the ICC temperature relative to the zero-birefringence temperature, and $T_{2\pi}$ is the temperature shift required to yield $\phi = 2\pi$. Using a 795 nm probe laser, we measured $T_{2\pi} = 4.5$°C. Thus the post-selected biphoton from our cavity-enhanced down-converter should change from a triplet, which occurs at zero time-bin difference ($m = 0$), to a singlet when $mT = T_{2\pi}/2$.

Data were collected for a series of ICC temperatures, so that the signal and idler resonated at different cavity lengths. Figure 3 shows the results for $T \approx 0.53$°C. The upper curve in this figure is the H-V histogram, and the filled curve is the $\pm 45^\circ$ histogram. As in Fig. 2, the central ($T = 0$) peak in the H-V histogram is suppressed in the $\pm 45^\circ$ histogram. For $T \neq 0$, however, the $\pm 45^\circ$ coincidence rate shows the $\sin^2$ oscillation expected from our $R_{\pm 45}(\tau)$ expression, with a period in m of 8.90 roundtrips (fit to the data). Thus the SPDC output was modulated between triplet and singlet signatures, with intermediate behavior occurring at roundtrip offsets in between these extremes. Their histogram ratio, shown in Fig. 5 curve B, clearly indicates the periodic change of the output state from triplet (ratio ~ 0.2) to singlet (ratio ~ 0.8).

Triplet behavior recurred whenever the temperature was detuned by a multiple of 4.5°C. The data for Fig. 4 were taken at $T = 2.26$°C with $\phi = \pi$. Now, all the even-roundtrip peaks are suppressed and all the odd-roundtrip peaks are maxima. The ratio alternates between a maximum and minimum—see Fig. 5 curve C—in agreement with the predicted period of 2 for this temperature detuning. The odd-roundtrip peaks are exhibiting polarization singlet behavior. The reduced contrast was due to detector time jitter, which causes the counts from one peak to spill into time bins associated with adjacent peaks. This effect also reduced the contrast in Fig. 5 curve B.

The ∼17% pump reflection from the output coupler lead to down-conversion in the backward pump path in Fig. 1. However, the ECC had the wrong orientation for pairs generated by this backward pump, thus they always produce a $\pm 45^\circ$-basis to H-V-basis ratio of 1/2, which reduced our measured quantum-interference visibility. We rotated the ECC by 90°, so that the forward-pump pairs have a 1/2 ratio and the backward pairs exhibit quantum interference. With this arrangement the $\pm 45^\circ$-basis to H-V-basis ratio for the $T = 0$ peak increased from 12%, for the normal-ECC orientation, to 43%, for the rotated-ECC orientation, indicating that 90% of the down-conversion was producing interference either forward or backward. Taking into account the ECC's 5 mm length not being exactly half the length of

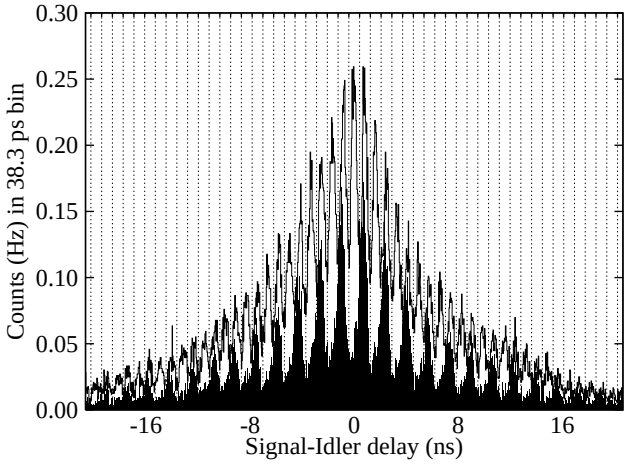

FIG. 4: Similar to Fig. 2 with the temperature detuned by 2.26°C.

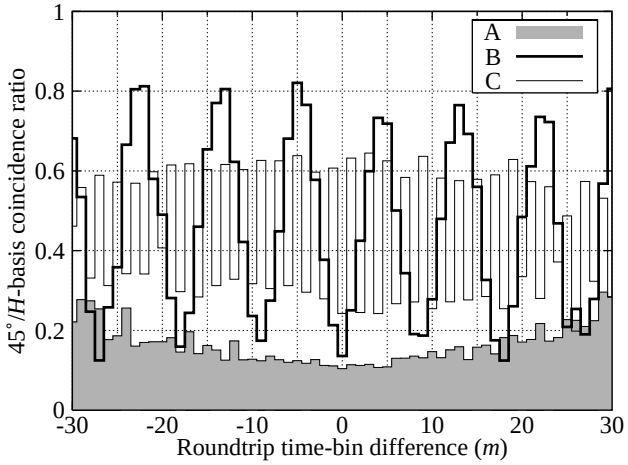

FIG. 5: Ratio of histograms from Figs. 2 (fill A), 3 (curve B), and 4 (curve C) versus roundtrip time-bin difference m.

the 9.7 mm PPKTP crystal, this is expected to be 93.2% for a matched ECC. The depths of the forward and backward dips imply that 18.6% of the pump was reflected, in agreement of the 17% estimate from the transmission measurements. The remaining 6.8% contrast loss comes from unknown sources of signal-idler distinguishability.

The peak TT-TR coincidence rate, during the cavity sweep, for the light collected by the single-mode fiber was 2000 pairs/s per mW of pump power. Because of the 50-50 beam splitter, this is 25% of the pairs from the fiber and 50% of the coincidence rate between the transmitted and reflected sides of the beam splitter. This rate is higher than the 300 pairs/(s-mW) obtained from this PPKTP crystal without cavity enhancement and without fiber coupling [6]. From the 280 GHz phase-matching bandwidth, 1.21 GHz FSR, and cavity finesse of 55, the FWHM of the central frequency peaks should be ∼22 MHz and should contain about 1/250 of the total output. It follows that our experiment produced 0.7 polarization-entangled pairs/s per mW of pump power per MHz of bandwidth at frequency degeneracy. These are pairs from a single fiber-coupled spatial mode, and are post-selected after a 50/50 beam splitter. In comparison, the single-pass source in Ref. [6] produced only 0.001 pairs/(s-mW-MHz) and the sources in Refs. [6, 7] produced 0.003 pairs/(s-mW-MHz) and 0.014 pairs/(s-mW-MHz), respectively. The type-I cavity-enhanced source in Ref. [4] used a $KbNO_3$ crystal and produced 0.12 pairs/(s-mW-MHz).

In summary, we have demonstrated cavity-enhanced type-II phase-matched SPDC producing spectrally bright, fiber-coupled polarization-entangled biphotons that are suitable for efficient coupling to narrowband atomic absorption lines. We have generated a novel biphoton state of time-bin modulated polarization entanglement that can be controlled by adjusting the cavity birefringence. The pure triplet biphoton state can only be obtained at zero birefringence. This unique property suggests that it may be potentially useful for ultrasensitive detection of weak intracavity birefringence. For example, one may place a normally isotropic material under thermal stress or piezoelectric strain in a zero-birefringence cavity-enhanced biphoton source. Any stress-induced material birefringence would induce a coincidence-rate modulation signature that yields the amount of the material birefringence.

Acknowledgments

This work was supported by a DoD MURI program under ARO-administered Grant No. DAAD-19-00-1-0177.

[1] P. G. Kwiat, K. Mattle, H. Weinfurter, A. Zeilinger, A. V. Sergienko, and Y. Shih, Phys. Rev. Lett. **75,** 4337 (1995); P. G. Kwiat, E. Waks, A. G. White, I. Appelbaum, and P. H. Eberhard, Phys. Rev. A **60,** R773 (1999); F. König, E. J. Mason, F. N. C. Wong, and M. A. Albota, Phys. Rev. A **71,** 033805 (2005); M. Fiorentino, C. E. Kuklewicz, and F. N. C. Wong, Opt. Express **13,** 127 (2005).

[2] J. H. Shapiro and N. C. Wong, 2002, J. Opt. B: Quantum Semiclass. Opt. **2,** L1 (2002).

[3] Z. Y. Ou and Y. J. Lu, Phys. Rev. Lett. **83,** 2556 (1999).

[4] H. Wang, T. Horikiri, and T. Kobayashi, Phys. Rev. A **70,** 043804 (2004).

[5] C. E. Kuklewicz, Ph.D. thesis, Massachusetts Institute of Technology, 2005.

[6] C. E. Kuklewicz, M. Fiorentino, G. Messin, F. N. C. Wong, and J. H. Shapiro, Phys. Rev. A **69,** 013807 (2004).

[7] M. Fiorentino, G. Messin, C. E. Kuklewicz, F. N. C. Wong, and J. H. Shapiro, Phys. Rev. A **69,** 041801(R) (2004).